



Effects of the STCC eddies on the Kuroshio based on the 20-year JCOPE2 reanalysis results



Yu-Lin Chang^{a,*}, Yasumasa Miyazawa^b, Xinyu Guo^c

^aNational Taiwan Normal University, Taiwan

^bJapan Agency for Marine-Earth Science and Technology, Japan

^cEhime University, Japan

ARTICLE INFO

Article history:

Received 14 October 2014

Received in revised form 12 March 2015

Accepted 20 April 2015

Available online 25 April 2015

ABSTRACT

In this study, 20 years of model reanalysis data are analyzed to study the effects of the subtropical countercurrent (STCC) eddies on the upstream Kuroshio, from east of Luzon to east of Taiwan. The effects are assessed from individual events to interannual time scales. The wind-driven Kuroshio is modified by the STCC eddies, with high spatiotemporal variations. The mass balance in the composite eddy events indicates that the strengthening and weakening of the Kuroshio transport are locally caused by the mass convergence and divergence produced by the eddies. The same analogy applies to the interannual time scale. In the eddy-rich years, the upstream Kuroshio is generally stronger because of wind forcing, yet the strengthening is nonuniform because of modification by the eddies. The larger number of warm eddies to the east of Taiwan and Luzon Island further strengthen the jet, whereas the larger number of cold eddies to the east of the Luzon Strait weaken the Kuroshio in the Luzon Strait. Drifter trajectories show larger Luzon Strait intrusion during the occurrence of cold eddies. The local weakening of the Kuroshio by cold eddies leads to a weaker potential vorticity jump, producing favorable conditions for the intrusion of a water mass into the South China Sea.

© 2015 Elsevier Ltd. All rights reserved.

Introduction

To the east of Taiwan and Luzon, a weak (a few cm s^{-1}) and shallow (~ 100 m) zonal current—the North Pacific subtropical countercurrent (STCC)—penetrates thousands of kilometers into the Pacific Ocean. The STCC was first observed by Uda and Hasunuma (1969) and later confirmed by White et al. (1978). The STCC is supported by subsurface density fronts produced by low potential vorticity mode water formed in the Kuroshio and Kuroshio Extension (Kobashi and Kubokawa, 2012). The STCC region is an enhanced eddy variability zone (Fig. 1), populated by eddies with typical diameters of 150–300 km and sea surface height (SSH) anomalies of ± 0.1 m (Chelton et al., 2011). The STCC eddies are spawned through baroclinic instability of the STCC and the North Equatorial Current system (Qiu, 1999). The sea surface temperature front in northern STCC also contributes to the growth of instability (Kobashi and Xie, 2012; Chang and Oey, 2014a). The eddies are distributed from the east of Taiwan to the dateline and from 17°N to 27°N (Chang and Oey, 2014b). Hwang et al. (2004) demonstrated that the movement of mesoscale eddies

near 22°N was ~ 8 km/day, based on TOPEX/Poseidon altimeter data. The STCC eddies propagate westward and approach the Kuroshio east of Taiwan and Luzon in a month to a year, depending on the locations at which the eddies are formed. The propagation direction can change when eddies encounter topography or interact with other eddies.

The Kuroshio is the western boundary current in the North Pacific Ocean. It flows through the area east of Luzon Island and Taiwan with a mean speed of 1–1.5 m/s (Nitani, 1972). The impact of eddies on the Kuroshio has been addressed in previous studies. Waseda et al. (2002) were one of the first to study the Kuroshio–eddy interaction using a high-resolution regional general circulation model. They revealed that mesoscale eddies to the southeast of Kyushu were associated with the Kuroshio meander to the south of Japan. Ebuchi and Hanawa (2003) found that the interaction between mesoscale eddies, for both anti-cyclonic and cyclonic eddies and the Kuroshio east of Kyushu, can sometimes trigger the Kuroshio meander south of Japan. Miyazawa et al. (2004) suggested that eddies further to the south (east of Taiwan and the Philippines) can affect the Kuroshio meander. Recent work by Soeyanto et al. (2014) indicated that the correlation between the Pacific Decadal Oscillation (PDO) index and the Kuroshio dropped significantly after 2002 because of the enhanced mesoscale eddies southeast of Taiwan.

* Corresponding author at: Institute of Marine Environmental Science and Technology, 88, Sec 4, Tingzhou Rd., Taipei 10677, Taiwan.

E-mail address: ychang@ntnu.edu.tw (Y.-L. Chang).

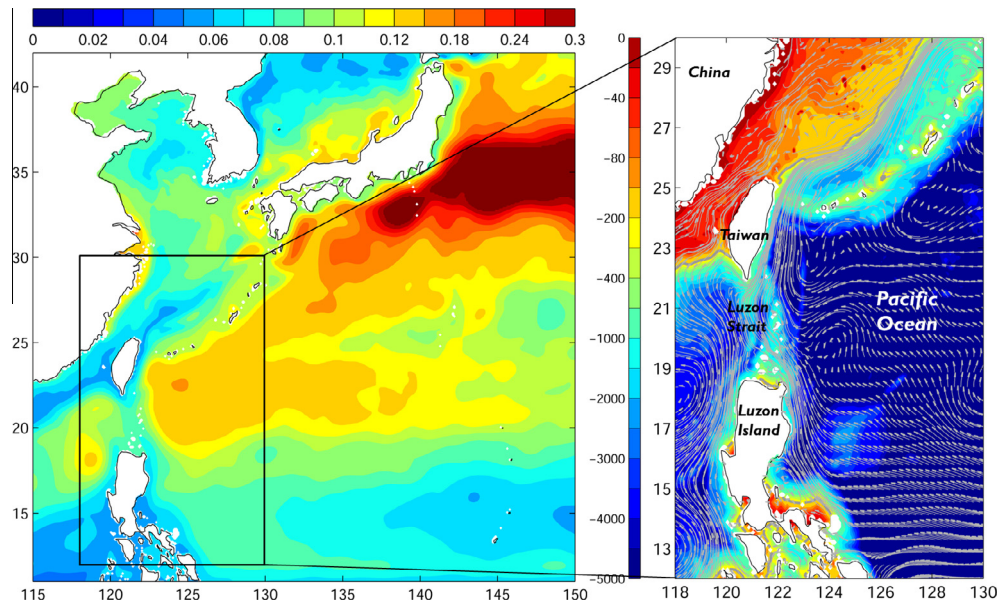


Fig. 1. Root-mean-squared SSH variability in the western North Pacific. SSH variability (m) is based on 20-year JCOPE2 data (left panel). Model bathymetry (m, color shading) is superimposed by the 20-year mean surface current trajectories (gray vectors, right panel). The right panel is a close-up of the domain in the black box in the left panel. (For interpretation of the references to colour in this figure legend, the reader is referred to the web version of this article.)

Although there is much evidence for the possible connection between eddies and the Kuroshio, classical theory suggests that the western boundary current obeys the Sverdrup dynamics. Sverdrup transport, controlled by large-scale wind stress curl, is mainly seasonal in the western Pacific subtropical gyre region. Based on the 20-month ADCP measurement, Johns et al. (2001) observed that the Kuroshio transport east of Taiwan fluctuated over a period of 100 days instead of seasonally. Recently, using the 29-year tide-gauge sea level difference as a proxy for Kuroshio transport, Chang and Oey (2011) revealed that the ensemble seasonal signal is barely significant and suggested a possible contribution of mesoscale eddy signals to the Kuroshio transport. STCC eddies, the origin of which could be associated with basin-scale water mass variability in the Western North Pacific (Kobashi and Kubokawa, 2012), are thought to be an important factor in modulating Kuroshio transport. Yang et al. (1999) demonstrated coherence between the tide gauge sea level difference (as a proxy for the Kuroshio) northeast of Taiwan ($\sim 25^\circ\text{N}$) and the SSH anomaly (SSHA) from satellite altimeter data. Zhang et al. (2001) concluded that the 100-day Kuroshio transport fluctuation observed by Johns et al. (2001) is related to STCC eddies. Using the cruise XBT/XCTD data from south of Taiwan ($21\text{--}22^\circ\text{N}$), Gilson and Roemmich (2002) observed that the Kuroshio geostrophic transport is reduced with the approach of the cyclonic eddies, while the warm eddies correspond to the strengthening of transport. The 8-year modeling simulation of Lee et al. (2013) showed that the Kuroshio transport variation east of Taiwan ($\sim 24^\circ\text{N}$) is related to the impinging eddies. Using observed 1-year mooring data, a recent study by Lien et al. (2014) suggested that the Kuroshio transport near the Luzon Strait (18.75°N) is modulated by the eddies. They found that the transport anomaly related to eddies can vary from 5 to 10 Sv ($1 \text{ Sv} = 10^6 \text{ m}^3 \text{ s}^{-1}$), with a temporal order of 10 days.

The possible link between the STCC eddies and the Kuroshio has been addressed in previous studies using observations and numerical simulations. In the earlier works, the Kuroshio transport was taken from a fixed section and a limited time period. Most of the results lead to the conclusion that warm eddies correspond to an increase in transport and cold eddies are related to transport reduction. However, results with the opposite conclusion have also

been reported (Zhang et al., 2001). In this work, we revisit this problem by extending the spatial and temporal scale based on the effective use of a recently produced comprehensive data product. Use of 20-year (1993–2012) eddy-resolving reanalysis data (JCOPE2; Miyazawa et al., 2009) allows us to perform intensive analysis of the entire upstream Kuroshio from east of Luzon Island to east of Taiwan for $\sim 1000 \text{ km}$ (Fig. 1), together with relevant mesoscale eddy activity. The longer temporal and larger spatial scales encompass more eddy events. By using composites of interannual and eddy events, we aim to obtain more general conclusions and to answer the following questions through the principle of mass balance. Does Kuroshio transport change with the presence of eddies? If so, how does the transport change? Why does the transport change? Are there spatial and temporal variations?

Data

JCOPE2 is a data-assimilated ocean model based on the Princeton ocean model, with a generalized coordinate system (Mellor et al., 2002). The domain encompasses the western North Pacific Ocean ($10.5\text{--}62^\circ\text{N}$, $108\text{--}180^\circ\text{E}$) with a horizontal resolution of $1/12^\circ$ and 46 vertical layers. The lateral boundary conditions are determined from the basin-wide model, using a one-way nesting method (Guo et al., 2003). The model is forced by wind stresses, heat, and salt fluxes from the six-hourly NCEP/NCAR reanalysis data. The AVHRR/MCSST, USGODAE project (<http://www.usgodae.org/>), CCAR Near Real-Time Altimetry Data (http://eddy.colorado.edu/ccar/data_viewer/index), and GTSP in situ temperature and salinity are assimilated into the model. Details of the model setup and descriptions can be found in Miyazawa et al. (2009).

The reduced-gravity (RG) model domain includes the North Pacific Ocean from 15°S to 70°N and from 99°E to 310°E . The horizontal resolution is 0.1° . The coastline is defined as the 200-m isobath. The RG model is forced by the NCEP/NCAR 6-hourly reanalysis wind, as used in JCOPE2. The simulation period is also the same as in JCOPE2, from 1993 to 2012. Parameters are given in Table 1. The RG model dynamics are dominated by wind-forced linear Rossby waves and Sverdrup balance. It does not have STCC eddies because of the inexistence of baroclinic instability. In this

Table 1
Parameters used in the North Pacific Ocean reduced-gravity model.

Parameter	Meaning	Value
g'	$g\Delta\rho/\rho$	0.02 m s^{-2}
H	Mean "upper-layer" depth	600 m
H_{coast}	Isobath where coastline is defined	200 m
α_N	Newtonian cooling coefficient	$1.25 \times 10^{-3} \text{ day}^{-1}$

work, the RG model is used to represent the wind-driven Kuroshio condition.

Results

The Sverdrup transport in the North Pacific Ocean is computed on the basis of the NCEP/NCAR reanalysis wind data. Fig. 2a shows the Sverdrup transport east of Taiwan at 23.2°N. The signal is led by seasonal variation with weak interannual variation; however, the seasonal signal is barely visible in the modeled Kuroshio transport (Fig. 2b). The Kuroshio penetrates to a depth of 600–800 m east of Taiwan (Johns et al., 2001) and is shallower (~500 m) east of Luzon Island (Qu et al., 1998). In this work, the Kuroshio transport is integrated vertically from the surface to $z = -600$ m, and horizontally from the defined western to eastern edges. The width (edge) of the Kuroshio is time-dependent. Apart from the fixed continental boundaries (Taiwan and Luzon Island), the edges of the Kuroshio are defined using its 0.1 m/s speed contours (Liang et al., 2003). The 20-year mean modeled transport east of Taiwan at 23.2°N is 20.4 Sv. This agrees with the 20-month observed mean transport of 21.5 Sv with 2.5 Sv uncertainty, as reported by Johns et al. (2001) using a 20-month moored current meter array east of Taiwan. The modeled Kuroshio transport shows a higher frequency variation than the seasonal signal from Sverdrup transport. The leading frequency is 80–100 days, according to the power spectra analysis. The ~100-day variability of the Kuroshio is closely associated with the STCC eddies (Zhang et al., 2001). Taking the upstream Kuroshio transport at 16.2°N, the correlation was performed with the downstream (northward) Kuroshio at any given latitude from 16.2°N to 25.8°N (Fig. 3) on an interannual time

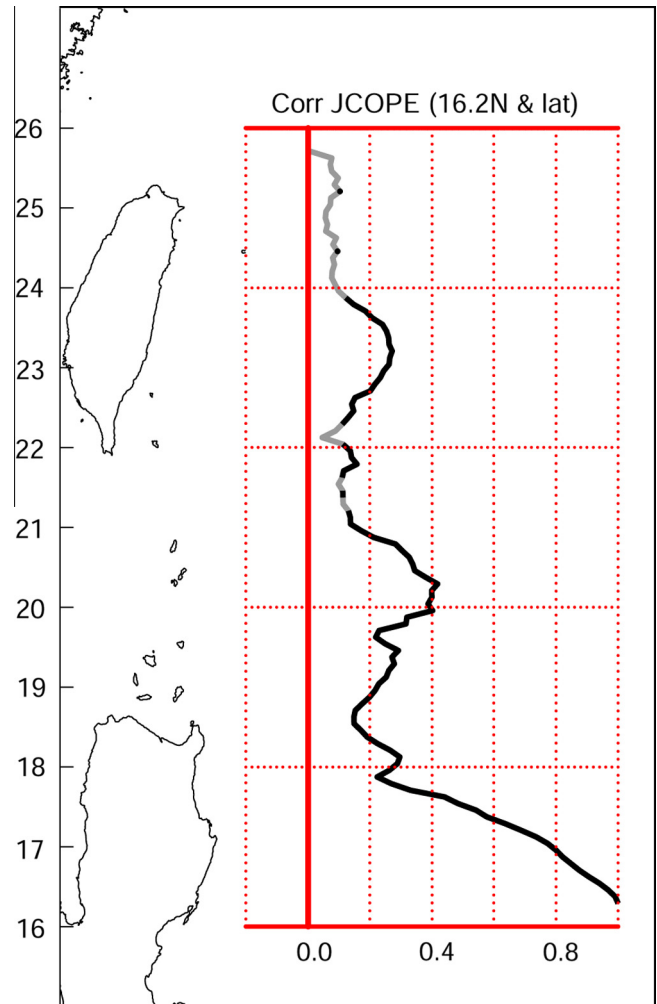


Fig. 3. Correlation coefficient between the Kuroshio transport (0–600 m) at a given latitude and that at 16.2°N from the model. Black lines indicate where the significance levels exceed 95%; gray lines are insignificant.

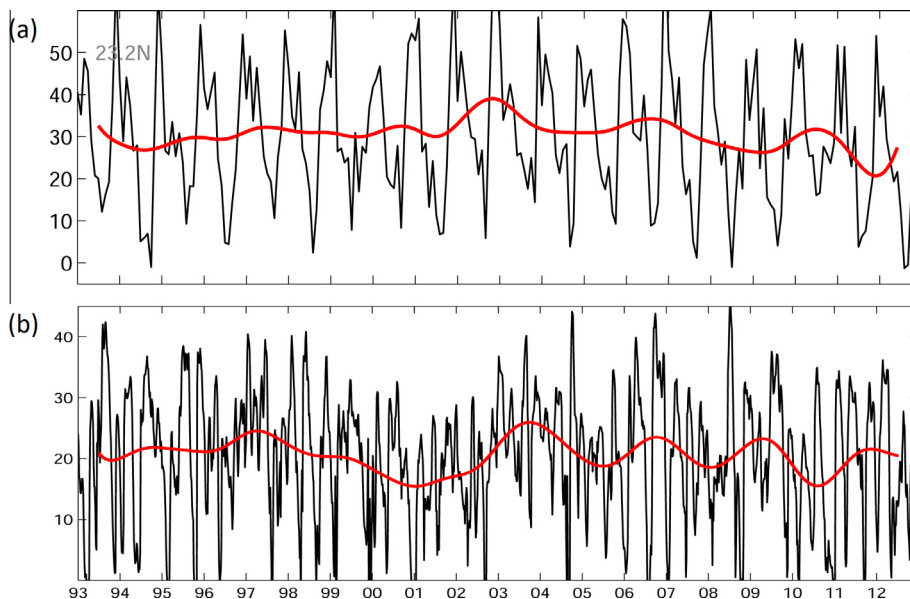


Fig. 2. Sverdrup and modeled Kuroshio transport. (a) NCEP/NCAR reanalysis of wind-derived Sverdrup transport at 23.2°N. (b) Modeled transport at 23.2°N. Superimposed red lines are the 360-day low-pass for interannual variation. The x-axis represents time in years; the y-axis represents transport in Sv. (For interpretation of the references to colour in this figure legend, the reader is referred to the web version of this article.)

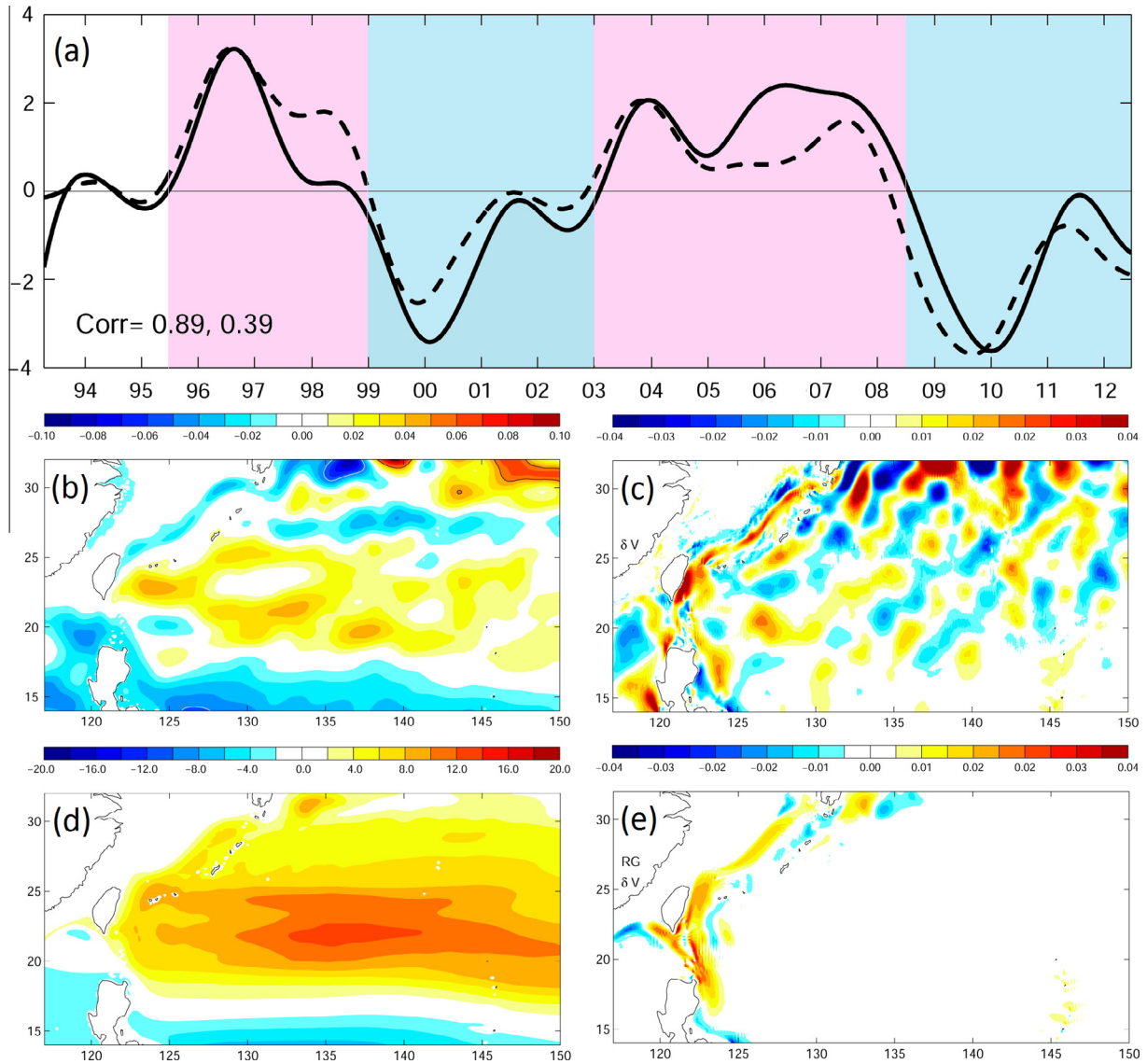


Fig. 4. (a) Eddy area anomaly for the model (solid line) and AVISO (dashed line). Red and blue shading indicate the eddy-rich and eddy-poor years, respectively. Numbers show the correlation coefficient and 95% significance level between the model and AVISO. The x-axis represents time, and the y-axis represents the area anomaly (%). Composites of eddy-rich years minus eddy-poor years for (b) SSH (m) from the 3D model; (c) 0–600 m mean meridional velocity (m/s) from the 3D model; (d) upper layer depth (m) from the RG model; and (e) meridional velocity (m/s) from the RG model. (For interpretation of the references to colour in this figure legend, the reader is referred to the web version of this article.)

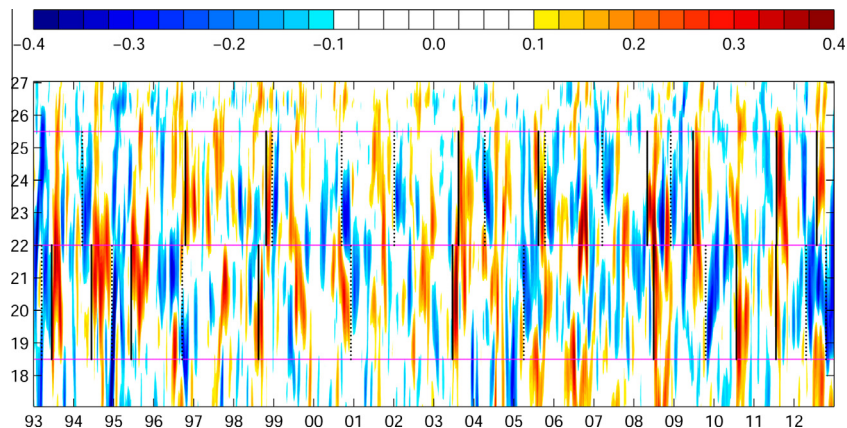


Fig. 5. SSHA at 125°E. SSHA are given in m. The x-axis represents time from 1993 to 2012; the y-axis represents latitude from 17°N to 27°N. Magenta lines mark the positions of the Luzon Strait (18.5–22°N) and Taiwan (22–25.5°N). Solid and dashed black lines denote the chosen warm and cold eddy events, respectively. (For interpretation of the references to colour in this figure legend, the reader is referred to the web version of this article.)

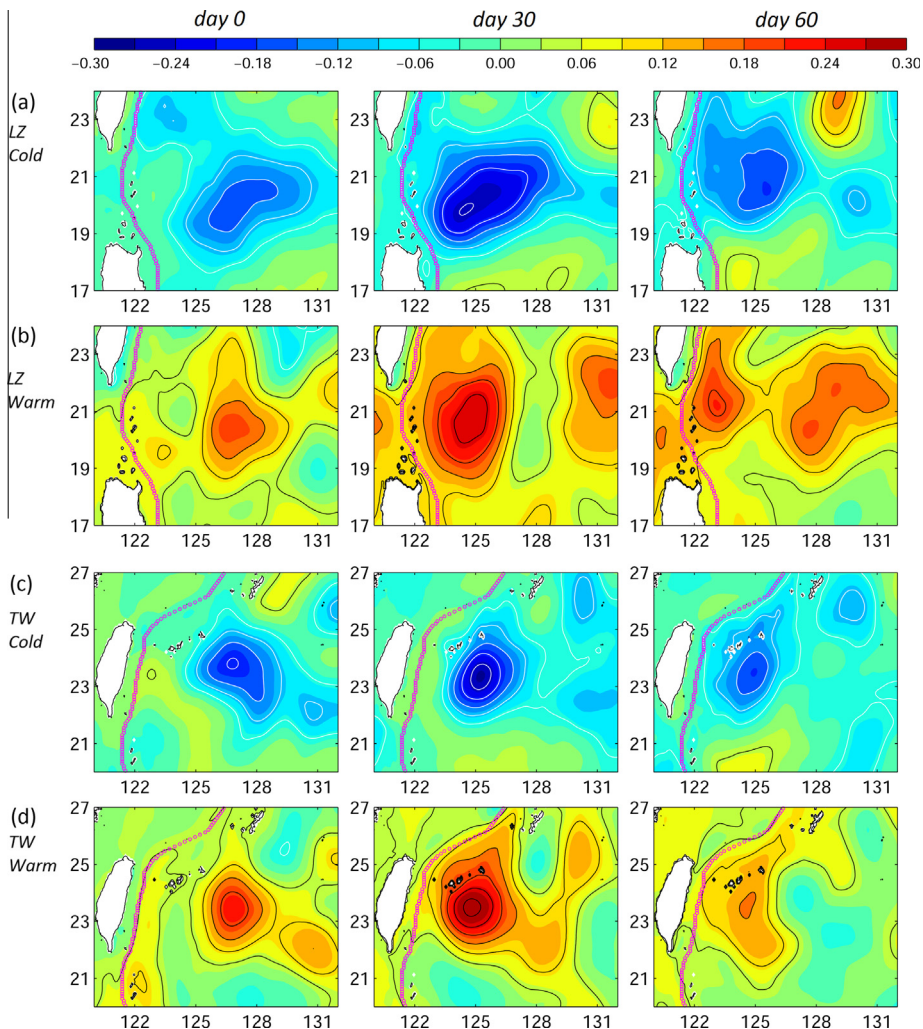


Fig. 6. Composite SSHA (m) based on the chosen eddy events for eddies to the east of the Luzon Strait (a and b) and for eddies to the east of Taiwan (c and d). (a and c) are cold eddies; (b and d) are warm eddies. From left to right, columns are Days 0, 30, and 60 after the eddy has passed through 125°E. The 20-year mean SSH is removed. Magenta dots indicate the chosen Kuroshio section that is used in Fig. 7. (For interpretation of the references to colour in this figure legend, the reader is referred to the web version of this article.)

scale (with a 360-day low-pass filter). The correlation coefficient rapidly dropped to ~ 0.2 downstream at $\sim 18^\circ\text{N}$ latitude, and remained low (< 0.4) further downstream. The subtropical wind gyre is on the scale of thousands of kilometers. If the Kuroshio is mainly wind-driven, a good correlation is expected within a distance of hundreds of kilometers on the interannual time scale. The Kuroshio transport variations diverge markedly from east of Luzon Island to east of Taiwan. The faster temporal and spatial changes of the Kuroshio indicate that the Kuroshio transport is not only driven by Sverdrup dynamics but is also affected by other factors such as eddies.

The Okubo–Weiss method (Okubo, 1970; Weiss, 1991) is used to detect eddies (Chang and Oey, 2014b). The Okubo–Weiss parameter W is defined as

$$W = s_n^2 + s_s^2 - \omega^2 \quad (1)$$

where $s_n = \partial u / \partial x - \partial v / \partial y$ and $s_s = \partial v / \partial x + \partial u / \partial y$ are the normal and shear components of strain, respectively, and $\omega = \partial v / \partial x - \partial u / \partial y$ is the relative vorticity. The identification criterion for an eddy is a negative value of W , in which vorticity is the leading component relative to the two strain terms. Following Isern-Fontanet et al. (2006), an eddy is defined as a region in which the value of W is

smaller than a threshold W_0 ($-1.71 \times 10^{-12} \text{ s}^{-2}$), where $W_0 = -0.2\sigma_w$, and σ_w is the spatial standard deviation of W . After the eddies are identified, the eddy area (m^2) in the STCC region (130°E – 180°E , 17°N – 27°N) is first integrated and subsequently normalized by the sum of the STCC region to represent the eddy occupation in STCC region (P_{eddy} , %). The eddy occupation is calculated for both AVISO and the model (Fig. 4a). The interannual variation of eddy occupation is well represented by the model, with a high correlation between the model and satellite observations of 0.89 (95% significance level = 0.39). The model interannual variation of eddy occupation is similar to the leading empirical orthogonal function mode of the eddy kinetic energy from Qiu and Chen (2013) computed using satellite altimetry data. The STCC eddies covered 31.3% and 30.8% of the STCC region from AVISO and the model, respectively. The eddy-rich and eddy-poor years are defined as a positive P_{eddy} anomaly and a negative P_{eddy} anomaly, respectively (Fig. 4a). The eddy-rich years were mid-1995 to 1998 and 2003 to mid-2008; the eddy-poor years were 1999 to 2002 and mid-2008 to 2012. Weaker variation prior to mid-1995 was excluded from this work. We grouped the model variables according to the defined periods when assessing the difference between eddy-rich and eddy-poor years. Fig. 4b–d shows the composite difference between the eddy-rich years and the eddy-poor years for

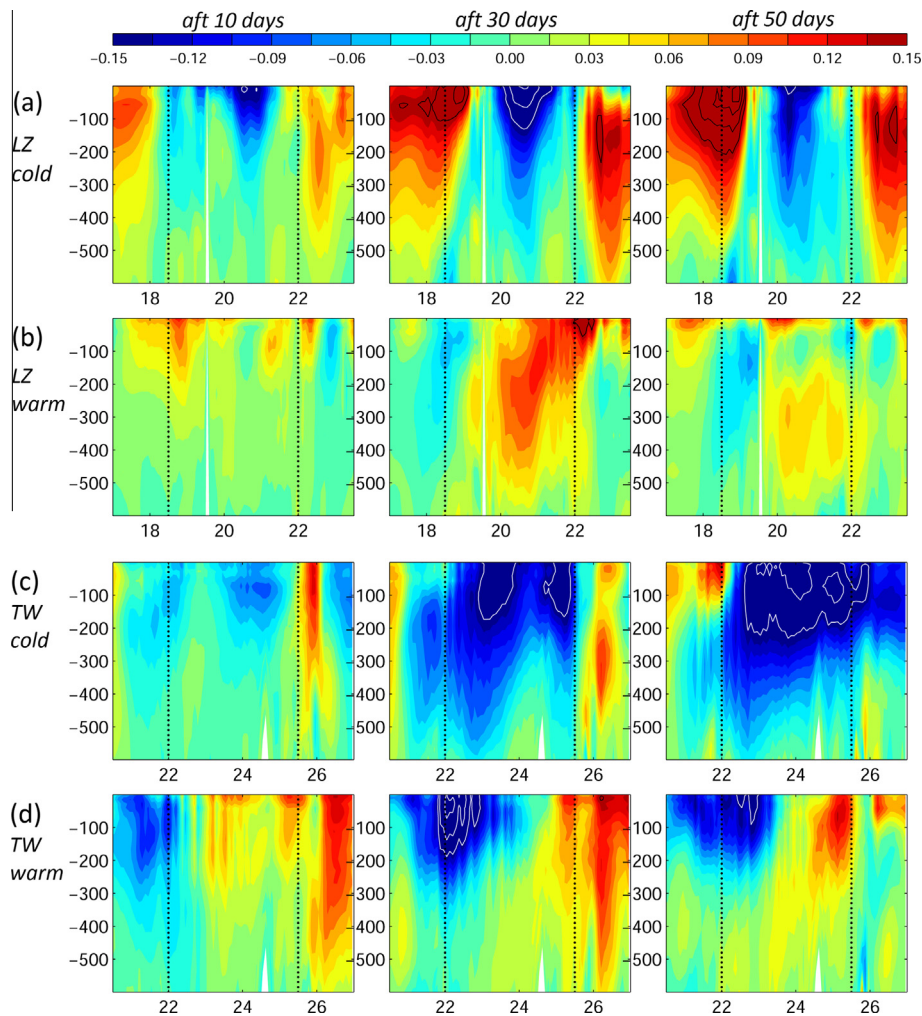


Fig. 7. Corresponding composite vertical profile of speed change along the Kuroshio path after eddies start to interact with the Kuroshio. Speed is defined as $(\sqrt{u^2 + v^2})$, m/s, and the Kuroshio path is shown by the dotted contour in Fig. 6. After 10 days (left), 30 days (middle), and 50 days (right). Black dotted lines mark the Luzon Strait (a and b), and Taiwan (c and d). Values that exceed the color scale are contoured. The contour interval is 0.05 m/s. The x -axis represents latitude; the y -axis represents depth in meters.

the three-dimensional (3D) model (JCOPE2) and the RG model. A positive SSH difference ($\Delta\eta$) with a circular shape is observed in the STCC region from the 3D model (Fig. 4b). This indicates that there are more warm eddies during the eddy-rich years than in the eddy-poor years (17.2% vs 15.2%, with significance >99%). The 0–600 m mean meridional velocity difference (Δv) is positive in the upstream Kuroshio from east of Luzon Island to east of Taiwan (Fig. 4c). The velocity difference in the upstream Kuroshio between the eddy-rich and the eddy-poor years accounts for 15–20% of mean velocity. Strengthening of the jet during the eddy-rich years is consistent with previous findings (Chang and Oey, 2011). However, the stronger Kuroshio during the eddy-rich years is not necessarily controlled by the eddies: the wind-driven dynamic included in the 3D model should also be considered. The composite is repeated for the RG model to check the effect of wind. The upper layer depth difference (ΔULD) in the STCC region is positive (Fig. 4d). The mesoscale circular shape structure vanished because of the inexistence of eddies in the RG model. A stronger Kuroshio with positive meridional velocity difference (Δv_{RG}) is also observed (Fig. 4e). Chang and Oey (2012) suggested that the eddy-rich years correspond to a positive Philippines–Taiwan Oscillation (PTO) when the subtropical wind stress curl is highly negative. The stronger subtropical wind stress curl forces a stronger subtropical gyre ($\Delta\text{ULD} > 0$), leading to a stronger Kuroshio ($\Delta v_{\text{RG}} > 0$) during the

eddy-rich years. The wind forcing explains the strengthening of the Kuroshio during the eddy-rich years.

There is a spatial difference between the 3D model and the RG model (Fig. 4c and e). The wind-forced strengthening of the Kuroshio is strongest near the Luzon Strait (Fig. 4e); however, the strongest enhancement in the 3D model is observed east of Taiwan (Fig. 4c), and Δv near the Luzon Strait is not as distinct as that to the east of Taiwan. The discrepancy between the 3D and RG model suggests that STCC eddies may play a role in modifying the Kuroshio strength.

The Kuroshio and eddies

Fig. 5 plots the SSHA at 125°E with time, in which abundant eddies are visible in the STCC area near the Kuroshio. The eddies are widely distributed in time and space. To analyze the effect of eddies on the Kuroshio, we first subdivided the domain meridionally into east of the Luzon Strait (18.5°N–22°N) and east of Taiwan (22°N–25.5°N). Grouping eddies geographically can help to avoid spatial signal cancelation. The composite was based on those eddies that passed through 125°E. Stronger eddies were chosen as a composite for each subdomain: eight warm eddies (solid lines in Fig. 5) and eight cold eddies (dashed lines in Fig. 5). Thirty-two eddies in total were sorted into four sets: warm and cold eddies

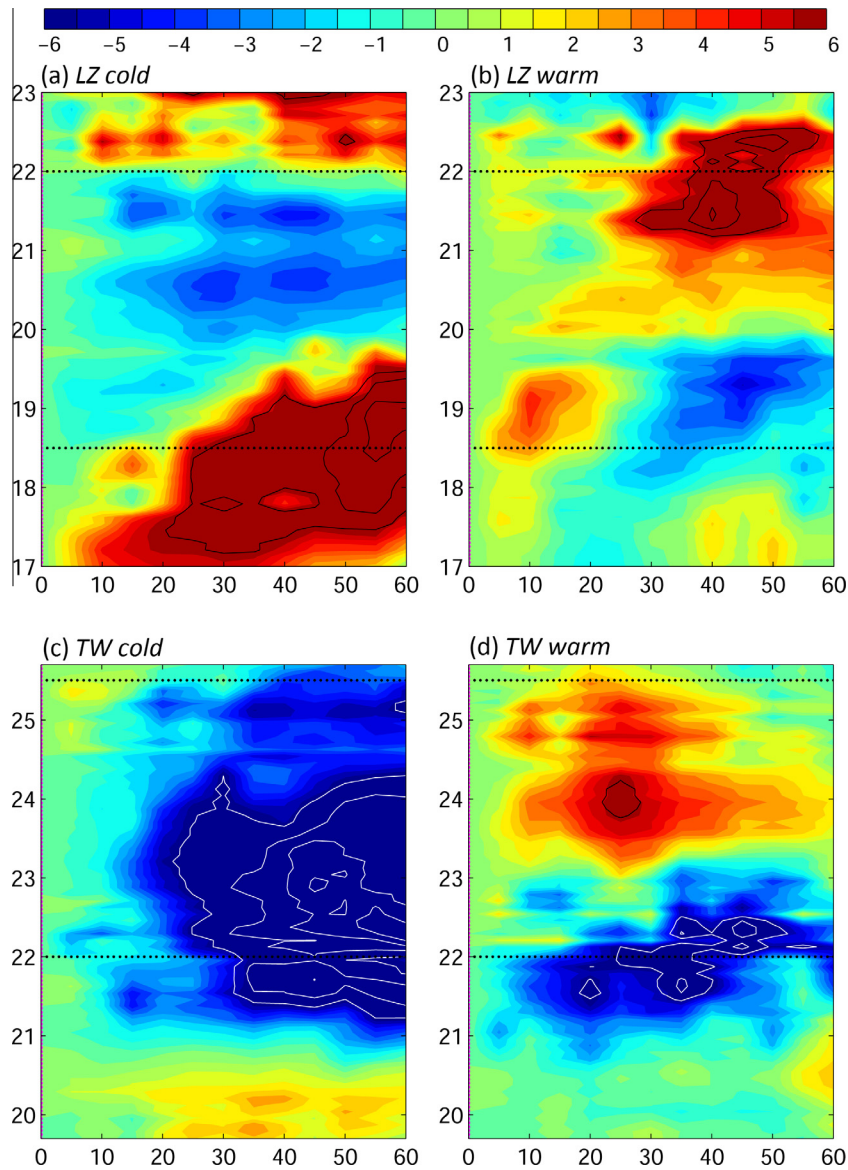


Fig. 8. Corresponding composite change in Kuroshio transport after eddies start to interact with the Kuroshio. Kuroshio transport is for 0–600 m depth, in Sv. Values that exceed the color scale are contoured. The contour interval is 2 Sv. The x-axis represents time in days; the y-axis represents latitude. (For interpretation of the references to colour in this figure legend, the reader is referred to the web version of this article.)

near Taiwan and the Luzon Strait. Fig. 6 shows composites of the SSHA (20-year mean removed) for Days 0, 30, and 60 after eddies pass through 125°E. On Day 30, the edges of the eddies arrive at ~122.5°E (Fig. 6a, b, and d). The composite cold eddy east of Taiwan moves more slowly (Fig. 6c), reaching ~123°E on Day 30. On Day 60, the western edge of the eddies remains at ~122°E, where the eddies weaken and are advected northward by the Kuroshio. To the east of the Luzon Strait, eddies are carried toward southern Taiwan (Fig. 6a and b), and eddies east of Taiwan are moved toward the East China Sea shelf (Fig. 6c and d).

The time axis is redefined in the following analysis. The dates when the edges of the eddy (0.1-m SSH contour) meet the eastern edge of the Kuroshio (0.1-m/s speed contour) are defined as Day 0. A section along the Kuroshio was chosen (dots in Fig. 6) to illustrate the effect of eddies on the Kuroshio. Fig. 7 shows the corresponding vertical profile of the speed ($\sqrt{u^2 + v^2}$) anomaly along the chosen section on Days 10, 30, and 50 after the eddy starts to interact with the Kuroshio. The Kuroshio speed on Day 0 is subtracted. The Kuroshio responds differently to warm and cold eddies

after the eddies start to interact with the jet. The Kuroshio becomes weaker when affected by the cold eddies (Fig. 7a and c) and is strengthened by the warm eddies (Fig. 7b and d). The interaction time of the eddies and the Kuroshio is around 50 days. The change in the Kuroshio speed reaches 0.2–0.25 m/s on Day 30 in the upper 200 m. The effect of eddies on the Kuroshio can penetrate to $\sim z = -600$ m. Notably, a speed anomaly with the opposite sign is also observed to the north/south of the composite area. In the case of the cold eddy east of Luzon Strait (Fig. 7a), the decrease in the Kuroshio speed is sandwiched by a positive anomaly to its north and south. The increase in the Kuroshio speed corresponds to the warm eddies to the north and south of the Luzon Strait (Fig. 6a). Similarly, in the case of the warm eddy east of Taiwan (Fig. 7d), the observed negative speed anomaly is associated with the cold eddy south of Taiwan (Fig. 6d).

A single chosen section is by itself insufficient to represent the overall Kuroshio. The corresponding composite Kuroshio transport is demonstrated in Fig. 8. The Kuroshio transport is computed following the same definition as used in Fig. 2b. Again, Day 0 of

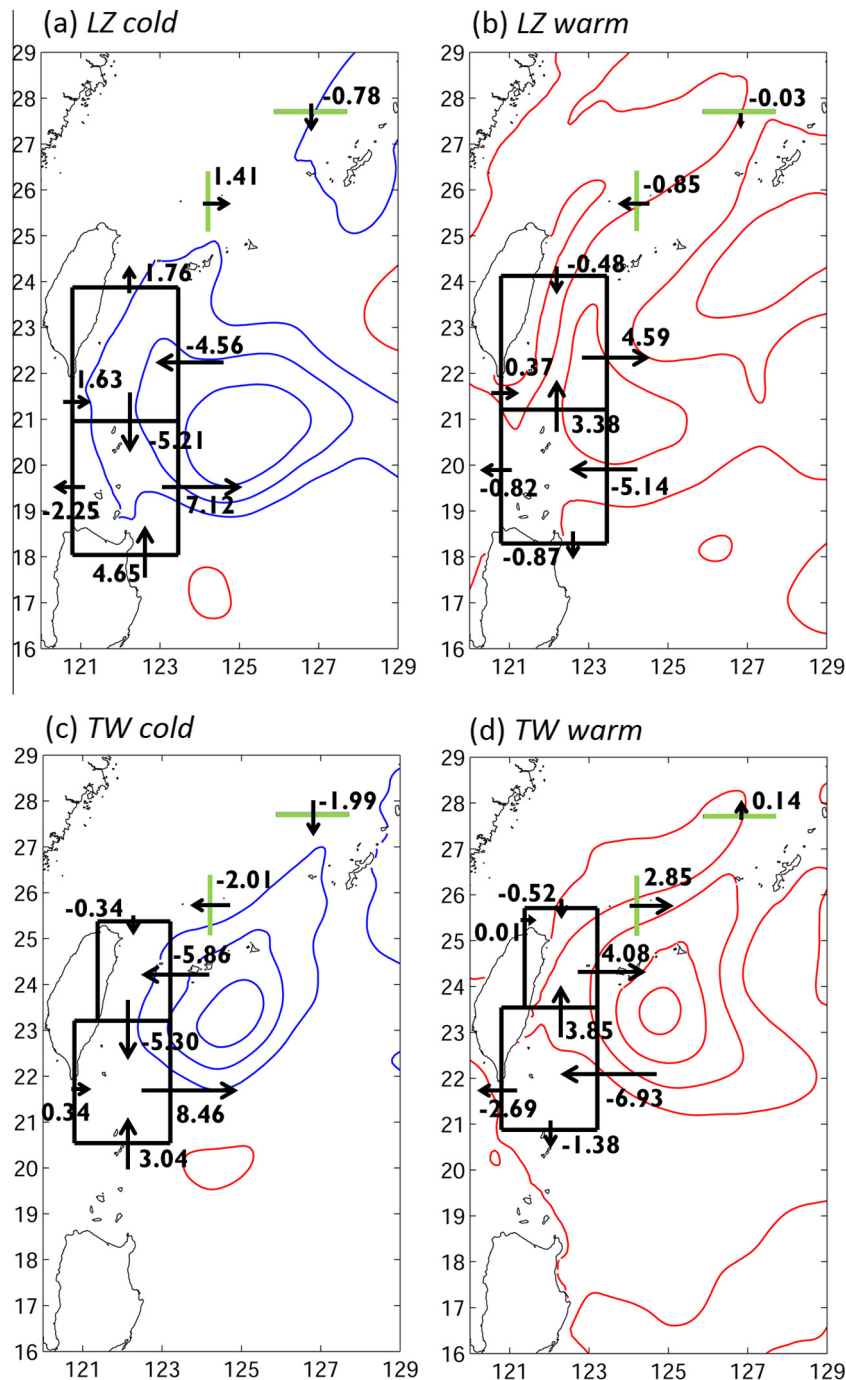


Fig. 9. Schematic plot for corresponding composite volume transport balance. Units are Sv. Color contours are SSHA: red for positive, blue for negative. The contour interval is 0.05 m. (For interpretation of the references to colour in this figure legend, the reader is referred to the web version of this article.)

the anomaly is when the eddy starts to interact with the Kuroshio (similar to that in Fig. 7). The changes in transport are large between Day 10 and Day 50. The effect of the eddy on the Kuroshio can last for more than 50 days until the eddy dissipates, advects, or joins the Kuroshio. The transport anomaly is 3–10 Sv. Transport variation relating to eddies accounts for 20–50% of Kuroshio mean transport (20.7 Sv, Fig. 2b). The results show that the cold eddies correspond to a decrease in Kuroshio transport, and warm eddies are associated with an increase in transport. In the transport composite, the transport anomaly north/south of the target area can also vary with the opposite sign, as observed for the speed profile (Fig. 7).

Why does the Kuroshio transport change?

The STCC eddies are nonlinear. The nonlinear feature is determined by the metric $U/c > 1$, where U is the maximum circum-averaged gyrotory speed within the eddy interior and c is the translation speed of the eddy (Chelton et al., 2011). The estimated U/c from the model in the STCC region is 2–4 and can sometimes reach 6–7. The nonlinearity implies that there is trapped fluid within the eddy interior (Flierl, 1981). Both warm and cold eddies carry mass. One may expect that as the eddy approaches the Kuroshio the eddy mass is merged into the jet. The Kuroshio transport should increase for both warm and cold eddies. However, the

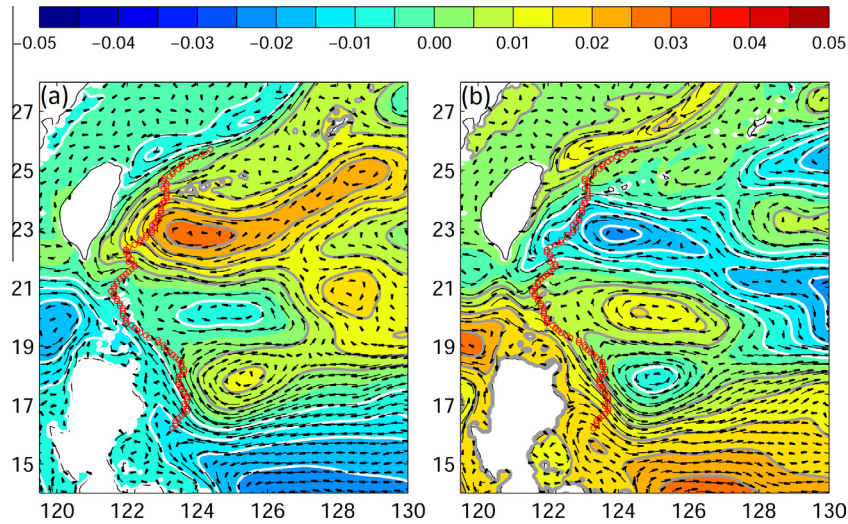


Fig. 10. Composite SSHA. SSHA are in m for (a) eddy-rich years, and (b) eddy-poor years. Black trajectories indicate the model surface current anomalies. Red dots indicate the 20-year mean Kuroshio eastern edge. (For interpretation of the references to colour in this figure legend, the reader is referred to the web version of this article.)

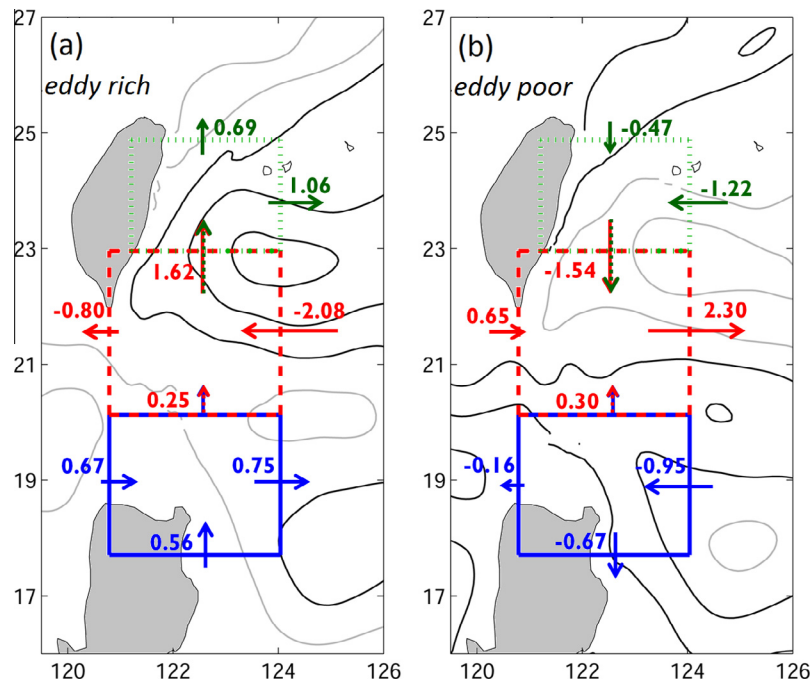


Fig. 11. Schematic plot for corresponding composite volume transport balance. (a) Eddy-rich years. (b) Eddy-poor years. Contours are SSHA: black for positive, gray for negative. The contour interval is 0.01 m.

results reveal that the Kuroshio responds differently to warm and cold eddies. Why does the Kuroshio transport decrease in the case of the cold eddy? In the case of the warm eddy, is the increase in Kuroshio transport maintained entirely in the downstream? Analysis of mass balance is performed to answer these questions. The same composite cases are used. The transports are computed along the given sections (Fig. 9). Two boxes are chosen in each composite case. One box is located southwest of the eddy, and the other is chosen to be northwest of the eddy. The two boxes can, therefore, show how the Kuroshio transport changes upstream and downstream of the eddy. The transport is again integrated for 0–600 m. The box is not completely closed, with an open boundary at $z = -600$ m. The transport is averaged from Day 10 to Day 60 after the eddy begins to interact with the Kuroshio. The transport

anomalies are referred to Day 0 (similar to that in Figs. 7 and 8). Fig. 9 shows a schematic plot of the mass balance. The mass balance shows that the Kuroshio transport changes nonuniformly in space. In the case of the cold eddy, the Kuroshio transport decreases west of the eddy; however, the upstream and downstream Kuroshio transport increase or are nearly unchanged (Fig. 9a and c). The condition is reversed in the case of the warm eddy (Fig. 9b and d). The spatial nonuniform Kuroshio transport is due to the mass convergence and divergence influenced by the eddy. The cold eddy produces mass convergence to its north (downstream of the jet) and divergence to its south (upstream of the jet), leading to a decrease in the Kuroshio transport. The warm eddy rotates in the opposite direction, resulting in mass convergence in the south and divergence to the north, leading to an

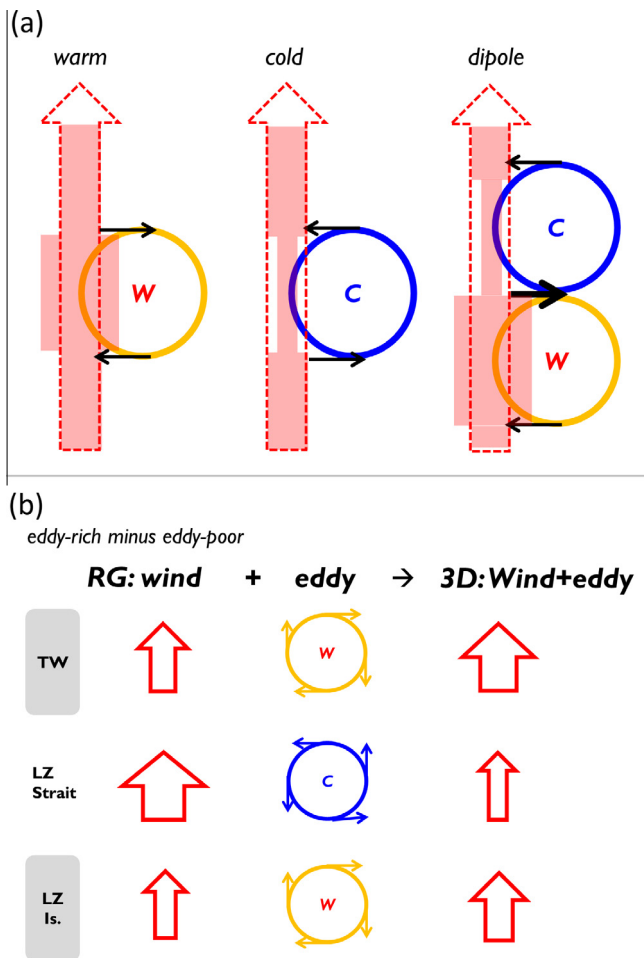


Fig. 12. Schematic plots of (a) how eddies influence the Kuroshio transport. The dashed red arrow represents the original state. Pink shading indicates the transport after eddy influence on the Kuroshio; and (b) how eddies modify the Kuroshio from wind-driven dynamics for eddy-rich years minus eddy-poor years. Gray rectangular boxes denote the relative locations of Taiwan (TW) and Luzon Island (LZ Is). The left panel represents the wind-driven reduced-gravity (RG) Kuroshio (Fig. 4e), the middle panel is the composite eddy (Fig. 10a minus Fig. 10b), and the right panel shows the Kuroshio from the 3D model (Fig. 4c). The wider the arrow, the larger the Kuroshio transport. Cold eddies are drawn in blue; warm eddies in gold. (For interpretation of the references to colour in this figure legend, the reader is referred to the web version of this article.)

increase in the Kuroshio transport. A warm eddy is observed to the south of the cold eddy (Fig. 9a and c), forming a dipole structure. The dipole eddies produce 8–9 Sv transport change in 200–300 km, resulting in strong divergence between the two eddies (southern box in Fig. 9a and c).

In addition, two more sections along the Kuroshio (Fig. 1b) in the East China Sea are chosen (green lines in Fig. 9) to check the effect of eddies on the downstream Kuroshio. For eddy cases of the Luzon Strait (Fig. 9a and b), the Kuroshio in the East China Sea is affected by separate local events. The increase (decrease) of transport in the southern (northern) section is due to the local warm (cold) eddies (Figs. 9a, 6a, and 8a). For eddy cases east of Taiwan, the southern section is affected by the same composite eddy event east of Taiwan, which results in a response similar to the eastern section of the northern box (Fig. 9c and d). The northern sections are not influenced by the same eddies east of Taiwan. This regional dependence has been addressed by Soeyanto et al. (2014). They found that the Kuroshio transport in the southern East China Sea depends on the STCC eddies, while the transport in the northern East China Sea is related to the eddies from north-east of the Okinawa Islands.

The western sections are located in the Luzon Strait. For the Luzon Strait (Fig. 9a and b), the total transport (south plus north) at the Luzon Strait is similar for both warm and cold eddy cases. For the individual section, larger mass fluxes are observed in the case of cold eddies (Fig. 9a) than for warm eddies (Fig. 9b). The cold eddy weakens the Kuroshio east of Luzon Strait. The weakening western boundary current tends to form a westward loop when it meets the gap (Sheremet, 2001). The larger mass flux in the case of the cold eddy implies that the Kuroshio loops into the South China Sea more than in the case of the warm eddy. Further details pertaining to this subject will be discussed in a later section.

How do eddies affect the Kuroshio in the eddy-rich and the eddy-poor years?

A difference between the 3D and RG models in terms of strengthening of the Kuroshio is noticed (Fig. 4). The difference can be explained by the eddies. The interesting tri-pole eddies are shown in the SSHA composite (Fig. 10). During the eddy-rich years, warm eddies are observed to the east of Taiwan and east of Luzon Island, while a cold eddy appears to the east of the Luzon Strait (Fig. 10a). This indicates that more warm eddies appear to the east of Taiwan and Luzon Island, and more cold eddies arrive east of the Luzon Strait during the eddy-rich years. The situation is reversed during the eddy-poor years. To demonstrate how eddies modify the Kuroshio transport from the wind-driven dynamics, the transport balance analysis is repeated for the eddy-rich and eddy-poor years (Fig. 11). The Kuroshio transport anomaly is referred to the 20-year mean transport. Three boxes are constructed to examine the change in the Kuroshio transport caused by the eddies. The interannual composite SSHA is weaker than the composite chosen eddies (approximately a quarter of the strength of the stronger cases; Figs. 10 and 6). The composite transport changes are therefore weaker; however, the results are consistent with the composite cases (Figs. 11 and 9). The Kuroshio transport is strengthened by the wind more during the eddy-rich years than during the eddy-poor years (RG model, Fig. 4). The Kuroshio transport varies spatially in response to the eddies. During the eddy-rich years, a cold eddy to the east of the Luzon Strait is sandwiched by warm eddies to its north and south. The convergence and divergence produced by these eddies enhance the Kuroshio transport to the east of Taiwan and Luzon Island, and reduce the transport to the east of the Luzon Strait. The reverse applies during the eddy-poor years (Fig. 11b). Schematic plots of how the eddies influence the Kuroshio for individual cases and how eddies modify the Kuroshio from the wind-driven dynamic for the composite difference between the eddy-rich and eddy-poor years (Figs. 4 and 10, respectively) are shown in Fig. 12.

Effect of eddies on the Kuroshio in the Luzon Strait

The effect of the local weakening of the Kuroshio transport in the Luzon Strait by cold eddies is demonstrated using modeled drifter trajectories. The same composite events are used. Drifters are released at 125°E, from 18.5°N to 22°N, at $z = -[0, 25, 50, 100, 200, 300, 400 \text{ m}]$, and tracked for 90 days. Drifters are tracked horizontally using the scheme of Awaji et al. (1980). Drifters for warm and cold eddy cases are sorted separately. The drifter trajectories are composited into one map and called the visitation frequency (VF). The VF represents the frequency of the drifter arrival for each grid. The VF shows both the path and frequency of the drifters' trajectories. Fig. 13 shows the composite VF for warm and cold eddies at the surface, $z = -100 \text{ m}$, and $z = -200 \text{ m}$. Drifters in the warm eddy cases are unable to travel from the Pacific Ocean to the South China Sea (Fig. 13, right panel). Conversely, composite

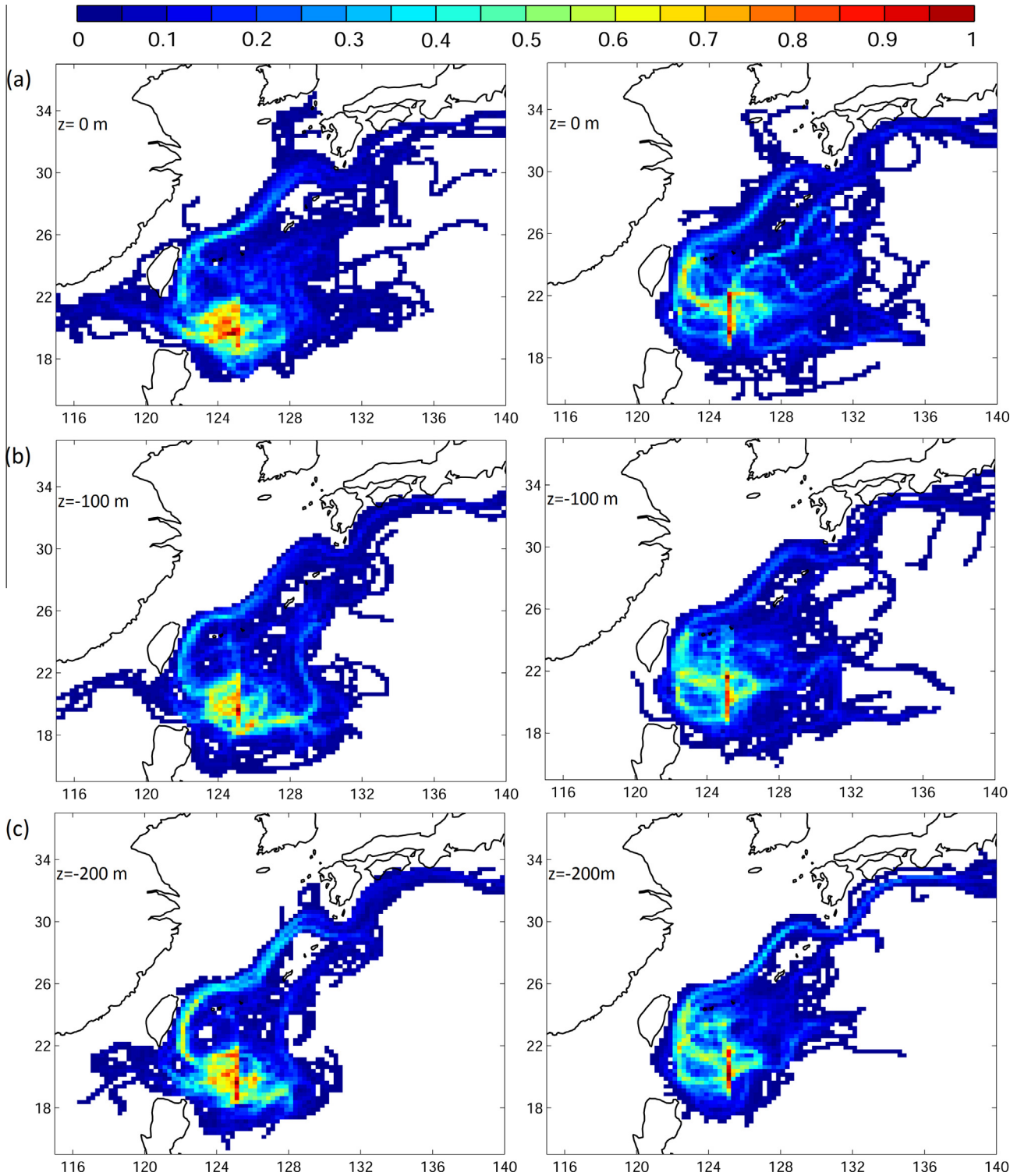


Fig. 13. Composite visitation frequency. Left panels show cold eddy cases, right panels show warm eddy cases, at (a) $z = 0$ m, (b) $z = -100$ m, and (c) $z = -200$ m. The unit is time normalized by 100.

cold eddy cases show clear Luzon Strait intrusion (Fig. 13, left panel). Similar phenomena are observed at each depth. The cold eddies weaken the Kuroshio transport east of the Luzon Strait (Fig. 9a). The larger mass fluxes in the Luzon Strait imply looping of the Kuroshio (Fig. 9a). Sheu et al. (2010) suggested that when the Kuroshio weakens, it tends to form a westward loop in the Luzon Strait and exhibits a weaker potential vorticity jump across

the jet. The weaker jet interacts with the eddies, resulting in a westward vector due to their mutually induced velocity. In such cases, the eddies are likely to propagate westward, entering the South China Sea. This applies to both warm and cold eddies. The potential vorticity (PV) is defined as

$$PV = \frac{\partial \rho}{\partial z} (f + \zeta) \quad (2)$$

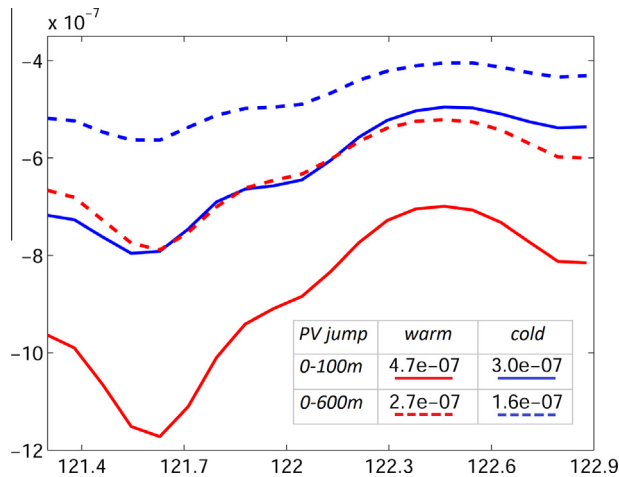


Fig. 14. Composite 0–100 m (solid lines) and 0–600 m (dashed lines) mean PV for warm (red) and cold (blue) eddy events in the Luzon Strait (mean from 19.5°N to 22°N) for the mean from Day 10 to Day 60 after the eddy interacts with the Kuroshio. The x-axis represents longitude. The values shown in table are the PV jump: the unit is $\text{m}^{-1} \text{s}^{-1}$. (For interpretation of the references to colour in this figure legend, the reader is referred to the web version of this article.)

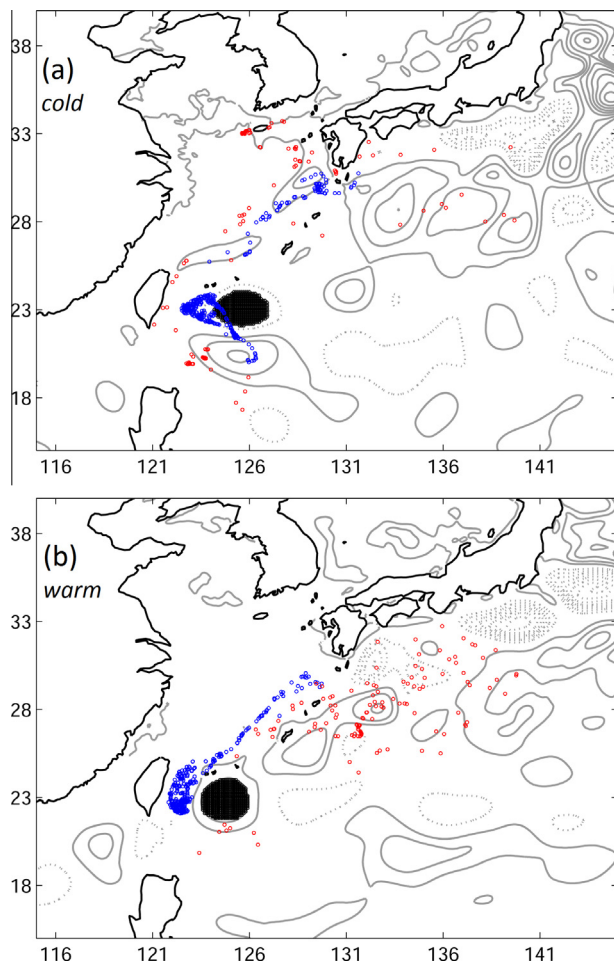


Fig. 15. Drifter distribution for (a) cold and (b) warm eddies on Day 0 (black), Day 40 (blue), and Day 140 (red). Gray contours show the SSHA on Day 0. Positive values are shown by solid contours; negative values are dotted. (For interpretation of the references to colour in this figure legend, the reader is referred to the web version of this article.)

where ρ is the density, f is the Coriolis parameter, and ζ is the relative vorticity. The PV jump is the PV change across the jet. The PV is again composited according to the selected eddy events, using the mean from 19.5°N to 22°N and from Day 10 to Day 60. The PV is plotted across the Kuroshio in the Luzon Strait for warm and cold eddy cases (Fig. 14). Vertical averaging was performed over 0–100 m, where the Kuroshio shows a larger change, and 0–600 m. The PV jump is weaker for cold eddies than for warm eddies, indicating more favorable conditions for intrusion during the former. The values of the 0–100 m (0–600 m) mean PV jump from Day 10 to Day 60 for warm and cold eddies were 4.7×10^{-7} (2.7×10^{-7}) and 3×10^{-7} (1.6×10^{-7}) $\text{m}^{-1} \text{s}^{-1}$, respectively. The local weakening of the Kuroshio by cold eddies generates favorable conditions for drifters to penetrate the Kuroshio and enter the South China Sea. The looping of the Kuroshio, along with the stronger westward intrusion, increases water exchange between the Pacific Ocean and the South China Sea. The same reasoning can also be applied to the interannual composite (Figs. 10 and 11).

Summary and discussion

The effect of eddies on the upstream Kuroshio was analyzed using the 20-year JCOPE2 reanalysis data. The change in Kuroshio transport is locally influenced by eddies caused by mass convergence and divergence. The warm eddies enhance the strength of the Kuroshio because of upstream convergence and downstream divergence. Conversely, cold eddies tend to weaken the Kuroshio because of the opposite rotation direction of the eddy. The same analogy applies to a composite of the eddy-rich and eddy-poor years. During the eddy-rich years, more warm eddies occur to the east of Taiwan and Luzon Island, whereas the east of the Luzon Strait is dominated by cold eddies. The convergence and divergence produced by the triple eddies modify the Kuroshio transport from wind-driven dynamics. The strongest Kuroshio observed to the east of the Luzon Strait in the wind-driven RG model is weakened by cold eddies, while the Kuroshio velocities to the east of Taiwan and east of Luzon Island are strengthened by warm eddies. This distribution is reversed during the eddy-poor years.

Local weakening of the Kuroshio in the Luzon Strait by cold eddies leads to a weaker PV jump across the jet. The weaker PV jump in the case of cold eddies allows greater intrusion into the South China Sea, increasing the water exchange between it and the Pacific Ocean.

The effect of the eddy on the Kuroshio transport is local. However, the eddy signal may be carried downstream. An example is given in Fig. 15 using drifter tracking analysis (the same tracking scheme as Fig. 13) to track the path of drifters. The drifters are released inside the eddy where the absolute SSHA is larger than 0.2 m on Day 0, when the eddy starts to interact with the Kuroshio. A warm eddy event and a cold eddy event east of Taiwan are demonstrated. The analysis is repeated in other eddy cases. The results are similar, as illustrated in Fig. 15. In the case of the cold eddy on Day 40, the eddy becomes weaker and some of the drifters are still kept inside the eddy; however, others are advected toward the downstream Kuroshio in the East China Sea (Fig. 15a). On Day 140, the original eddy has disappeared as a result of dissipation. The distribution of drifters is no longer in circular shape, and some of the drifters are located to the south of Japan. Generally similar results are obtained in the warm eddy case (Fig. 15b). However, the details of the drifter dispersion appear complicated and could be affected by the chaotic advection activated by the eddy–Kuroshio interaction (Waseda and Mitsudera, 2002). This result implies that eddies in the upstream Kuroshio may propagate downstream, thus affecting the downstream

Kuroshio. The link between the eddies east of Taiwan and the large meander south of Japan was noticed by Miyazawa et al. (2004). Chang and Oey (2012) suggested that the STCC eddies may trigger the large meander south of Japan during the positive PTO phase (eddy-rich years). Other possible effects on the downstream Kuroshio are worth exploring.

This study demonstrates the mass flux in the Kuroshio region. The transport shows mass flux between the Kuroshio and the eddies. However, the water mass exchange between the Kuroshio and the eddies remains unclear. More detailed analyses including water mass variability and chaotic transport are needed to investigate the details of the eddy–Kuroshio interaction processes. Moreover, eddies can affect not only the mass transport but also the heat fluxes. Further study is required to understand how the warm and cold eddies change the Kuroshio heat fluxes and how this may affect the ecosystem.

Acknowledgments

The authors would like to acknowledge the AVHRR/MCSST, USGODAE project, CCAR Near Real-Time Altimetry Data, and the GTSP for providing data for model simulations. YLC is supported by the Ministry of Science and Technology of Taiwan under grant 102-2611-M-003-003-MY3. X.G. and Y.M. are supported by JSPS KAKENHI (26287116). Comments from reviewers were useful for improvements of the earlier versions of the manuscript.

References

- Awaji, T., Imasato, N., Kunishi, H., 1980. Tidal exchange through a strait: a numerical experiment using a simple model basin. *Journal of Physical Oceanography* 10, 1499–1508.
- Chang, Y.-L., Oey, L.-Y., 2011. Interannual and seasonal variations of Kuroshio transport east of Taiwan inferred from 29 years of tide-gauge data. *Geophysical Research Letters* 38, L08603. <http://dx.doi.org/10.1029/2011GL047062>.
- Chang, Y.-L., Oey, L.-Y., 2012. The Philippines–Taiwan oscillation: monsoon-like interannual oscillation of the subtropical–tropical western North Pacific wind system and its impact on the Ocean. *Journal of Climate* 25, 1597–1618.
- Chang, Y.-L., Oey, L.-Y., 2014a. Instability of the North Pacific subtropical countercurrent. *Journal of Physical Oceanography* 44, 818–833.
- Chang, Y.-L., Oey, L.-Y., 2014b. Analysis of STCC eddies using the Okubo–Weiss parameter on the model and satellite data. *Ocean Dynamics* 64 (2), 259–271. <http://dx.doi.org/10.1007/s10236-013-0680-7>.
- Chelton, D.B., Schlax, M.G., Samelson, R.M., 2011. Global observations of nonlinear mesoscale eddies. *Progress in Oceanography* 91, 167–216.
- Ebuchi, N., Hanawa, K., 2003. Influence of mesoscale eddies on variations of the Kuroshio path south of Japan. *Journal of Oceanography* 59, 25–36.
- Flierl, G.R., 1981. Particle motions in large-amplitude wave fields. *Geophysical and Astrophysical Fluid Dynamics* 18, 39–74.
- Gilson, J., Roemmich, D., 2002. Mean and temporal variability in Kuroshio geostrophic transport south of Taiwan (1993–2001). *Journal of Oceanography* 58, 183–195.
- Guo, X., Hukuda, H., Miyazawa, Y., Yamagata, T., 2003. A triply nested ocean model simulating the Kuroshio—roles of horizontal resolution on JEBAR. *Journal of Physical Oceanography* 33, 146–169.
- Hwang, C., Wu, C.R., Kao, R., 2004. TOPEX/Poseidon observations of mesoscale eddies over the subtropical countercurrent: kinematic characteristics of an anticyclonic eddy and a cyclonic eddy. *Journal of Geophysical Research* 109. <http://dx.doi.org/10.1029/2003JC002026>.
- Isern-Fontanet, J., García-Ladona, E., Font, J., 2006. Vortices of the Mediterranean Sea: an altimetric perspective. *Journal of Physical Oceanography* 36, 87–103.
- Johns, W.E., Lee, T.N., Zhang, D., Zantopp, R., 2001. The Kuroshio east of Taiwan: moored transport observations from the WOCE PCM-1 array. *Journal of Physical Oceanography* 31, 1031–1053.
- Kobashi, F., Kubokawa, A., 2012. Review on North Pacific subtropical countercurrents and subtropical fronts: role of mode waters in ocean circulation and climate. *Journal of Oceanography* 68, 21–43.
- Kobashi, F., Xie, S.-P., 2012. Interannual variability of the North Pacific subtropical countercurrent: role of local ocean–atmosphere interaction. *Journal of Oceanography* 68, 113–126.
- Lee, I.-H., Ko, D.S., Wang, Y.-H., Centurioni, L., Wang, D.-P., 2013. The mesoscale eddies and Kuroshio transport in the western North Pacific east of Taiwan from 8-year (2003–2010) model reanalysis. *Ocean Dynamics* 63, 1027–1040.
- Liang, W.-D., Tang, T.Y., Yang, Y.J., Ko, M.T., Chuang, W.-S., 2003. Upper ocean current around Taiwan. *Deep-Sea Research Part II* 50, 1085–1105.
- Lien, R.-C., Ma, B., Cheng, Y.-H., Ho, C.-R., Qiu, B., Lee, C.M., Chang, M.-H., 2014. Modulation of Kuroshio transport by mesoscale eddies at the Luzon Strait entrance. *Journal of Geophysical Research* 119, 2129–2142.
- Mellor, G.L., Hakkinen, S., Ezer, T., Patchen, R., 2002. A generalization of a sigma coordinate ocean model and an intercomparison of model vertical grids. In: Pinardi, N., Woods, J.D. (Eds.), *Ocean Forecasting: Conceptual Basis and Applications*. Springer, New York, NY, pp. 55–72.
- Miyazawa, Y., Guo, X., Yamagata, T., 2004. Roles of mesoscale eddies in the Kuroshio paths. *Journal of Physical Oceanography* 34, 2203–2222.
- Miyazawa, Y., Zhang, R., Guo, X., Tamura, H., Ambe, D., Lee, J.-S., Okuno, A., Yoshinari, H., Setou, T., Komatsu, K., 2009. Water mass variability in the western North Pacific detected in a 15-year eddy resolving ocean reanalysis. *Journal of Oceanography* 65, 737–756.
- Nitani, H., 1972. Beginning of the Kuroshio. In: Stommel, H., Yoshida, K. (Eds.), *Kuroshio: Its Physical Aspects*. University of Tokyo Press, Tokyo, Japan, pp. 129–163.
- Okubo, A., 1970. Horizontal dispersion of floatable particles in the vicinity of velocity singularities such as convergences. *Deep-Sea Research* 17, 445–454.
- Qiu, B., 1999. Seasonal eddy field modulation of the North Pacific subtropical countercurrent: TOPEX/Poseidon observations and theory. *Journal of Physical Oceanography* 29, 2471–2486.
- Qiu, B., Chen, S., 2013. Concurrent decadal mesoscale eddy modulations in the western North Pacific subtropical gyre. *Journal of Physical Oceanography* 43, 344–358.
- Qu, T., Mitsudera, H., Yamagata, T., 1998. On the western boundary currents in the Philippine Sea. *Journal of Geophysical Research* 103, 7537–7548.
- Sheremet, V., 2001. Hysteresis of western boundary current leaping across a gap. *Journal of Physical Oceanography* 31, 1247–1259.
- Sheu, W.-J., Wu, C.-R., Oey, L.-Y., 2010. Blocking and westward passage of eddies in the Luzon Strait. *Deep-Sea Research II* 57, 1783–1791.
- Soeyanto, E., Guo, X., Ono, J., Miyazawa, Y., 2014. Interannual variations of Kuroshio transport in the East China Sea and its relation to the Pacific Decadal Oscillation and mesoscale eddies. *Journal of Geophysical Research Oceans* 119, 3595–3616.
- Uda, M., Hasunuma, K., 1969. The eastward subtropical countercurrent in the western North Pacific Ocean. *Journal of the Oceanographical Society of Japan* 25, 201–210.
- Waseda, T., Mitsudera, H., 2002. Chaotic advection of the shallow Kuroshio coastal waters. *Journal of Oceanography* 58, 627–638.
- Waseda, T., Mitsudera, H., Taguchi, B., Yoshikawa, Y., 2002. On the eddy–Kuroshio interaction: evolution of the mesoscale eddy. *Journal of Geophysical Research* 107 (C8). <http://dx.doi.org/10.1029/2000JC000756>.
- Weiss, J., 1991. The dynamics of enstrophy transfer in two-dimensional hydrodynamics. *Physica D* 48, 273–294.
- White, W.B., Hasunuma, K., Solomon, H., 1978. Large-scale seasonal and secular variability of the subtropical front in the western North Pacific from 1954 to 1974. *Journal of Geophysical Research* 83, 4531–4544.
- Yang, Y., Liu, C.-T., Hu, J.-H., Koga, M., 1999. Taiwan Current (Kuroshio) and impinging eddies. *Journal of Oceanography* 55, 609–617.
- Zhang, D., Johns, W.E., Lee, T.N., Liu, C.-T., Zantopp, R., 2001. The Kuroshio east of Taiwan: modes of variability and relationship to interior mesoscale eddies. *Journal of Physical Oceanography* 31, 1054–1074.